AD-A183 626 THE ADSORPTION OF H2 AND D2 ON FE(110) 2 ANGLE RESOLVED 1/1
THERMAL DESORPTIO..(U) RENSSELAER POLYTECHNIC INST TROY
NY DEPT OF MATERIALS ENGINEE.. E A KURZ ET AL.
UNCLASSIFIED 30 JUL 87 TR-3 N00014-86-K-0259 F/G 7/2 NL

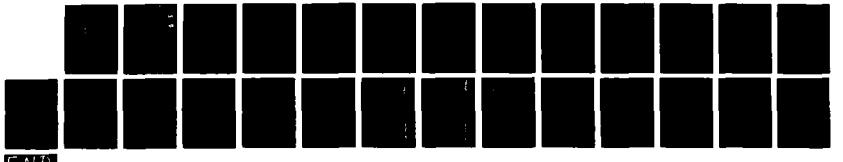

END
9-87
DTIC

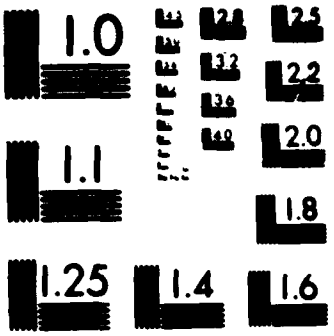

Unclassified

DTIC FILE COPY (12)

AD-A183 626 REPORT DOCUMENTATION PAGE

Unclassified	1b RESTRICTIVE MARKINGS
2a SECURITY CLASSIFICATION AUTHORITY	3 DISTRIBUTION / AVAILABILITY OF REPORT: Approved for public release; distribution unlimited
2b DECLASSIFICATION / DOWNGRADING SCHEDULE	
4 PERFORMING ORGANIZATION REPORT NUMBER(S): Technical Report #3	5 MONITORING ORGANIZATION REPORT NUMBER
6a NAME OF PERFORMING ORGANIZATION: Materials Engineering Dept. RPI	6b OFFICE SYMBOL (If applicable)
6c ADDRESS (City, State, and ZIP Code): Troy, NY 12180-3590	7a NAME OF MONITORING ORGANIZATION: Office of Naval Research
	7b ADDRESS (City, State, and ZIP Code): Chemistry Program, 800 N. Quincy Street, Arlington, VA 22217
8a NAME OF FUNDING / SPONSORING ORGANIZATION: Office of Naval Research	8b OFFICE SYMBOL (If applicable)
8c ADDRESS (City, State, and ZIP Code): Chemistry Program, 800 N. Quincy St., Arlington, VA 22217	9 PROCUREMENT INSTRUMENT IDENTIFICATION NUMBER: Contract # N00014-86-K-0259
	10 SOURCE OF FUNDING NUMBERS: PROGRAM ELEMENT NO. / PROJECT NO. / TASK NO. / WORK UNIT ACCESSION NO

DTIC ELECTE AUG 13 1987 D

11 TITLE (Include Security Classification)
"The Adsorption of H_2 and D_2 on Fe(110) II: Angle Resolved Thermal Desorption Spectroscopy and Kinetic Mechanism"

12 PERSONAL AUTHOR(S)
E.A. Kurz and J.B. Hudson

13a TYPE OF REPORT	13b TIME COVERED	14 DATE OF REPORT (Year, Month, Day)	15 PAGE COUNT
Interim Technical	FROM _____ TO _____	1987-7-30	23

16 SUPPLEMENTARY NOTATION
Submitted to Surface Science

17 COSATI CODES		
FIELD	GROUP	SUB-GROUP
		hydrogen

18 SUBJECT TERMS (Continue on reverse if necessary and identify by block number)
TEAS, Single Crystal Thermal Desorption

19 ABSTRACT (Continue on reverse if necessary and identify by block number)

Results of angle resolved thermal desorption spectroscopy (ARTDS) measurements for the adsorption of D_2 and H_2 on Fe(110) are presented. A detailed model of the interaction process has been developed using these results in combination with results obtained using thermal energy atom acattering (TEAS), reported in Part I of this work. ~~ARTDS~~ was used to measure the desorption flux as a function of surface polar angle during temperature programming following adsorption at a low temperature. Second order desorption kinetics, as observed with TEAS in part I, were confirmed. H_2 and D_2 were found to adsorb directly, dissociatively and with an activation energy for adsorption of 700 cal/mole. The sticking coefficient was observed to decrease with increasing coverage as $(1 - \theta)^2$ for θ greater than 0.1.

20 DISTRIBUTION / AVAILABILITY OF ABSTRACT	21 ABSTRACT SECURITY CLASSIFICATION
☒ UNCLASSIFIED/UNLIMITED ☒ SAME AS RPT ☐ DTIC USERS	Unclassified
22a NAME OF RESPONSIBLE INDIVIDUAL: Dr. David L. Nelson	22b TELEPHONE (Include Area Code): (202) 696-4410 / 22c OFFICE SYMBOL

DD FORM 1473, 84 MAR — 83 APR edition may be used until exhausted. All other editions are obsolete. SECURITY CLASSIFICATION OF THIS PAGE

87 8 6 006

OFFICE OF NAVAL RESEARCH

Contract N00014-86-K-0259

Task No. NR-056-533

TECHNICAL REPORT NO. 3

THE ADSORPTION OF H_2 AND D_2 ON Fe(110) II: ANGLE RESOLVED THERMAL DESORPTION SPECTROSCOPY AND KINETIC MECHANISM

by

E.A. Kurz and J.B. Hudson

Rensselaer Polytechnic Institute
Materials Engineering Department
Troy, New York 12180-3590

July 30, 1987

ABSTRACT

Results of angle resolved thermal desorption spectroscopy (ARTDS) measurements for the adsorption of D_2 and H_2 on Fe(110) are presented. A detailed model of the interaction process has been developed using these results in combination with results obtained using thermal energy atom scattering (TEAS), reported in Part I of this work. ARTDS was used to measure the desorption flux as a function of surface polar angle during temperature programming following adsorption at a low temperature. Second order desorption kinetics, as observed with TEAS in part I, were confirmed. H_2 and D_2 were found to adsorb directly, dissociatively and with an activation energy for adsorption of 700 cal/mole. The sticking coefficient was observed to decrease with increasing coverage as $(1 - \theta)^2$ for θ greater than 0.1.

1. INTRODUCTION

In this study we have applied two techniques to the investigation of the adsorption and desorption of both hydrogen and deuterium on Fe(110). These two techniques are thermal energy atom scattering (TEAS), as previously described in Part I of this work [1], and angle resolved thermal desorption spectroscopy (ARTDS). In this paper we present the results of the ARTDS study and show the detailed picture of the adsorption-desorption process that can be obtained from the combination of the two techniques.

Thermal desorption spectroscopy (TDS) is an experimental technique wherein the emission of a gas from an adsorbate-covered surface is monitored as the surface is heated. Redhead [2] has presented the basic mathematical and experimental techniques used in the study of simple desorption kinetics. The details of performance and analysis techniques of thermal desorption experiments have been greatly expanded on by many authors [3-5].

2. EXPERIMENTAL PROCEDURE

All thermal desorption experiments were performed utilizing the same ultra-high vacuum system and sample discussed in Part I of this work [1]. In all thermal desorption experiments, the iron crystal was cleaned as previously described, annealed and cooled to 200 K. The surface was monitored by AES before and after each set of TDS experiments and by specular helium scattering before each run. The sample was exposed to a given isotropic pressure of hydrogen or deuterium for a given time, to reach the desired exposure. The sample was then heated at a linear rate of 15 K per second through the range where desorption occurred. The

desorbing species was monitored by the mass spectrometer in the detector chamber. This mass spectrometer saw only those molecules which left the surface of the sample on a direct line of sight through two differentially-pumped orifices and into the ionizer. This eliminated any effects due to adsorption at the sample edge and uncleaned backside, as well as any desorption occurring from the sample support assembly. Due to the geometry of the ionizer and mass analyzer in the detector chamber and the high pumping speed in the chamber, any gas molecules which entered this chamber by passing directly through the two orifices, but were not ionized, made one unhindered pass through the detector and were then pumped away.

The sensitivity of the detector mass spectrometer was calibrated by introducing a known pressure of the desired gas into the main chamber and measuring the response of the detector mass spectrometer. The sensitivity was measured in this way after each desorption run.

Two types of TDS experiment were performed. In one set of measurements, the sample was first centered on and oriented perpendicular to the line of sight from the sample center to the ionizer. TDS spectra for various exposures of hydrogen and deuterium were obtained. In the other set of measurements, the sample was given a deuterium exposure of either 522 L or 6.5 L. Thermal desorption spectra were then recorded at various angles of the sample with respect to the line of sight from the sample to the ionizer.

3. RESULTS AND ANALYSIS

3.1 Angle Resolved Thermal Desorption Spectroscopy

In the first set of measurements, in which the sample was oriented

normal to the line of sight from the sample to the ionizer, deuterium thermal desorption experiments were performed for exposures ranging from 2L to 1500 L. Typical desorption spectra are shown in Figure 1. The temperature was measured by the thermocouple, the output of which is plotted on the X axis.

The spatial distribution of the desorbed deuterium was studied at exposures of 6.5 and 522 L. Typical desorption transients are shown in Figure 2. A plot of the desorption flux as a function of desorption angle normalized to the flux perpendicular to the surface, is shown in Figure 3. The 6.5 L and 522 L exposures exhibit identical behavior as a function of angle, and are well described by a $\cos^d \theta$ dependence where $d = 2.03 \pm 0.11$.

Desorption of molecules in equilibrium with the surface leads to a cos θ spatial desorption distribution. More peaked desorption patterns are an indication of an activation barrier for adsorption. As an approximation, it was assumed that molecules desorbing from a potential well which has an activation barrier for adsorption acquire an excess translational energy normal to the surface. Consider the qualitative effects of this excess translational energy upon the signal intensity measured by a density sensitive detector such as the mass spectrometer used in this study. Molecules desorbing normal to the surface will have a higher velocity than those desorbing at larger angles, and all will have velocities greater than in the case of equilibrium desorption. Thus, the observed intensity of all desorption spectra will be decreased by some amount from their true values. The amount of this decrease increases for desorption angles closer to the surface normal. Therefore, the overall effect of this excess energy is the underestimation of both the number of desorbed molecules and d, the exponent of the spatial distribution.

Coverages calculated from the raw TDS data yielded lower values than those obtained from helium scattering experiments performed under identical conditions. The saturation coverage calculated from the raw TDS data was lower than the accepted value of 1.7×10^{15} atoms / cm^2 [6]. It is thought that this discrepancy is due to the excess velocity of desorbed molecules, as discussed above. Unfortunately, there was no way to measure directly the velocity of the desorbed molecules in the present study. It was found that the addition of a small excess velocity normal to the surface, equivalent to $0.18\ \bar{v}$, where $\bar{v}$ is the mean molecular velocity at the desorption temperature, increased the saturation coverage calculated from the TDS data to 1.7×10^{15} atoms/cm^2. This velocity correction narrowed the spatial distribution from $\cos^{2.03}\theta$ to $\cos^{2.18}\theta$.

Figure 4 presents corrected desorption spectra for deuterium desorption along the surface normal for exposures ranging from 2L to 522L. Each spectrum is a smoothed average of three thermal desorption runs performed under identical conditions. Above about 8 L, a small peak begins to appear on the low temperature side of the deuterium desorption peak. Similar behavior has been observed in the adsorption of hydrogen on Fe(110), and has been attributed to a more weakly bound state arising from weak repulsive adsorbate-adsorbate interactions [6].

Figure 5 is a plot of deuterium coverage as a function of exposure at a surface temperature of 200 K, showing both the corrected ARTDS results and the HeTDS results described in Part I. This figure reveals excellent agreement between the two sets of data. Further evidence of this agreement is shown in Figure 6. Differentiation of the HeTDS data yields an independent measure of the desorption rate as a function of

temperature. The results of this process are shown as solid circles in the figure, the corresponding ARTDS data as X's.

These two sets of desorption transients are well described by the equation for second-order desorption with constant E_d and ν developed by Redhead [2], namely

$$(r_d)_p/r_d = \{\exp[-(E_d/2R)(1/T_p - 1/T)] + (T/T_p)^2[(E_d/2R)(1/T - 1/T_p)]\}^2 , \quad (1)$$

in which $(r_d)_p$ is the maximum valued r_d, the desorption rate.

The activation energy for deuterium desorption from the strongly bound state (when the second peak was not visible) was calculated by plotting $\ln(\sigma_0 T^2_p)$ versus $1/T_p$, where σ_0 is the initial coverage and T_p the temperature at which the desorption rate is a maximum. This plot was found to be linear, indicating second order desorption kinetics. The activation energy for desorption and second order pre-exponential were found to be $E_d = 27.3 \pm 1.8$ kcal/mole and $\nu = (5 \pm 2) \times 10^{-2}$ cm^2 / molecule sec, respectively.

3.2 Studies with Hydrogen

The range of exposures that could be studied in ARTDS measurements of adsorbed hydrogen was limited to exposures greater than 250 L by the presence of a high hydrogen background pressure in the detector chamber . The spatial distribution deduced from measurements as a function of polar angle, using the same type of velocity correction factor as was used for deuterium, was $\cos^{2.25\pm0.3}\theta$. Exposure to 1000 L of hydrogen at 200K yielded a saturation coverage of $(1.9\pm0.3) \times 10^{15}$ atoms/cm^2, within experimental error of the accepted value of 1.72×10^{15} atoms/cm^2.

3.3 Permeation Measurements

An additional set of experiments was performed which will be briefly described. In these experiments, hydrogen at atmospheric pressure flowed past the high pressure side of a thin iron crystal ((110) orientation) which was coated with palladium. The hydrogen dissociated and diffused through the crystal. Upon reaching the other side of the crystal, which was maintained in an ultrahigh vacuum system, the hydrogen reassociated and desorbed. This system has been described in detail elsewhere [7]. From 373K to 773K, the activation energy for permeation was found to be 8.16 kcal/mole, in good agreement with previous studies [8]. The spatial distribution of the desorbing hydrogen molecules was also monitored and exhibited a $\cos^{2.35} \theta$ dependence.

4. DISCUSSION

Differentiation of the coverage vs exposure data (Figure 5) yields the sticking coefficient as a function of coverage, $S(\theta)$. $S(\theta)$ is plotted vs $(1 - \theta)^2$ in Figure 7. The dependence of the sticking coefficient on $(1 - \theta)^2$ is similar to that previously reported [6]. In direct dissociative adsorption, each incident molecule must encounter two adjacent vacant sites in order to adsorb. Thus, for direct dissociative adsorption, the probability of adsorption is expected to be linearly dependent on $(1 - \theta)^2$. Figure 7 exhibits this linear dependence of the sticking coefficient on $(1 - \theta)^2$ for values of θ between 0.11 and 1.0. The curve deviates from linearity at low coverage. The cause of this deviation is uncertain, but may be due to the presence of a small number of surface defects, as proposed by Bozso [6]. These defect sites enhance the rate of adsorption at low coverage. The defect sites rapidly

saturate, and do not affect the remainder of the adsorption process. In addition, the rate of adsorption in direct dissociative adsorption is directly proportional to the molecular impingement rate and independent of the surface temperature. The initial sticking coefficient for direct dissociative adsorption is also independent of the surface temperature. This is exactly the observed behavior.

This enhanced rate of adsorption at low coverages due to defect sites is similar to the concept of "holes" in an activation barrier where non-activated adsorption may occur, as has been proposed by Comsa and David [9]. Indeed, step sites on close packed metal surfaces have been observed to exhibit non-activated hydrogen adsorption, whereas hydrogen adsorption on the close packed terraces is activated [10-12]. The "holes" in the Comsa and David model may correspond to defect sites on the surface where the activation barrier is reduced or nonexistent. Alternatively, the "holes" may be inherent in the energetic structure of the surface, as recently suggested by Karikorpi et al [13].

Assuming that the linear dependence of the sticking probability on $(1 - \theta)^2$ extends to zero coverage on those sites for which a barrier to adsorption exists, (as shown by the dashed line on Figure 7) leads to an initial sticking coefficient of 0.10 for direct dissociative adsorption on these sites. However, the actual initial sticking coefficient is greater than this value. This difference, 0.05, is the fraction of incident particles adsorbed through holes in the activation barrier, either inherent or associated with defects. The Comsa and David model predicts that the spatial distribution of the desorbed molecules will obey the following relation:

$$N(\theta')/N(0) = \frac{(1-r)(1+X/\cos^2\theta')[\exp(-X/\cos^2\theta')]+r}{(1-r)(1+X)[\exp(-X)]+ r} [\cos\theta'] \qquad (2)$$

where r is the fraction adsorbed without activation, X is E_a/kT (E_a is the activation barrier for adsorption), N(0) is the number of molecules desorbed normal to the surface, and N(θ') is the number desorbed at some angle, θ', with respect to the surface normal. Fitting the observed thermal desorption spatial distribution to this equation, with r = 0.05, yields an activation barrier for adsorption, E_a, of 710 ± 80 cal/mole.

The spatial distribution was also fit to the Van Willigen [14] model which states that,

$$N(\theta')/N(0) = \frac{E_a+kT\cos^2\theta'}{(E_a+kT)\cos\theta'} \{\exp[-(E_a/kT)\tan^2\theta']\} \qquad (3)$$

where all parameters are as previously described. (Note that if r = o in the Comsa model, it reduces to the Van Willigen model.) This yields a value of 580 ± 70 cal/mole for the activation barrier. As expected, this is close to the value predicted by the Comsa and David model, since r is small.

The slightly lower value of E_a predicted by the Van Willigen model is consistent with the concept of non-activated adsorption occurring at a small number of sites. Molecules desorbing from these non-activated sites should exhibit a cos θ spatial distribution, whereas those desorbed from activated sites should exhibit a narrower distribution. The Comsa model separates the two effects, while the Van Willigen model assumes a uniform

surface. However, since the surface is [illegible] non-activated sites broadens the spatial distribution of desorbed molecules, the value of E_a calculated using the van Willigen model

Similar calculations were performed for the data obtained by the permeation technique. Activation barriers of 870 ± 90 cal/mole and 980 ± 110 cal/mole were calculated using the van Willigen model and the Gomsa model ($r = 0.05$), respectively. The activation barriers calculated from the permeation data are consistently greater than those calculated from the ARTDS data. This may be due to the relative cleanness of the samples. The cleanness of the permeation sample was monitored by AES alone, whereas the cleanness of the TDS sample was monitored by both AES and helium beam specular scattering. Differences in surface cleanness probably exist between these two surfaces, and contaminants have been shown to narrow the desorbed spatial distribution and hence increase the apparent activation energy for adsorption.

The heats of adsorption determined for hydrogen (24.2 kcal/mole) and deuterium (24.7 kcal/mole) adsorption using TEAS are in reasonable agreement with the previous work of Wedler et al. [15], who have investigated hydrogen and deuterium adsorption on polycrystalline iron films. The difference between the two values is also in qualitative agreement with theoretical harmonic oscillator calculations which yield a deuterium zero point energy 1.8 kcal/mole lower than that calculated for hydrogen. The lower zero point energy for deuterium is consistent with the slightly smaller scattering cross section observed for deuterium as compared to hydrogen. However, a meaningful evaluation of this dependence cannot be performed from the data obtained in the present study, as the scattering cross sections for hydrogen and deuterium are well within a

standard deviation of each other.

It should also be noted that the measured values of the activation energy for desorption, E_d, consistently exceed the corresponding heats of adsorption, ΔH_a, by roughly 1 kcal/mol. This difference is consistent with the calculated values for the activation energies for adsorption, as

$$E_d = \Delta H_a + E_a. \tag{4}$$

The extent to which this relation can be quantitatively demonstrated in the present work is limited by experimental uncertainty.

5. CONCLUSIONS

The thermodynamic and kinetic parameters determined in this study, and the methods used to determine them, are summarized in Table 1. Figure 8 shows the potential energy diagram deduced from this study. The following conclusions were drawn from this study of hydrogen and deuterium adsorption on Fe(110).

1. Hydrogen and deuterium adsorb dissociatively on Fe(110).
2. Adsorption is activated. An activation barrier for adsorption of 710 cal/mole is predicted by the Comsa and David model. On the surface examined in this investigation, approximately 5% of the atoms are adsorbed through a non-activated process, possibly at or near defect sites.
3. Adsorption proceeds by direct dissociative adsorption into the chemisorbed atomic state without trapping in a molecular precursor state.

4. The initial sticking coefficients of hydrogen and deuterium on Fe(110) were measured to be 0.18 and 0.15, respectively. For both gases, the sticking coefficient was linearly dependent on $(1 - \theta)^2$ when θ was between 0.1 and 1.0.

ACKNOWLEDGMENTS

This research was supported in part by the Office of Naval Research under Contract Number N00014-86-K-0259. Information contained in this paper does not necessarily reflect the position of the government; no official endorsements should be inferred. This paper is based on a thesis presented by one of us (EAK) in partial fulfillment of the requirements for the Ph. D. degree in Materials Science.

REFERENCES

1. E.A. Kurz and J.B. Hudson, Surface Sci., in press
2. P.A. Redhead, Vacuum, 12 (1962), 203.
3. D.A. King, Surface Sci., 47 (1975), 384.
4. R.J. Madix, Chemistry and Physics of Solid Surfaces, Vol. II, Ed. R. Vanselow, CRC Press, Inc., 1979.
5. R.B. Anderson, P.T. Dawson, Eds., Experimental Methods in Catalytic Research, Vol. 3, Academic Press, New York, 1976.
6. F. Bozso, G. Ertl, M. Grunze, and M. Weiss, Appl. Surface Sci., 1 (1977), 103.
7. E. Kurz, Ph.D. Thesis, Rensselaer Polytechnic Institute, Troy, NY, 1986.
8. R.F. Miller, J.B. Hudson, and G.S. Ansell, Met. Trans. A, 6A (1975), 117.
9. G. Comsa, and R. David, Chem. Phys. Lett., 49 (1977), 512.
10. H. Kurner, M. Luger, H.P. Steinruck, A. Winkler, and K.D. Rendulic, Surface Sci. 163 (1985), L 641.
11. R.J. Gale, M. Salmeron, and G.A. Somorjai, Phys. Rev. Lett., 38 (1977), 1027.
12. H.J. Robota, W. Bielhaber, M.C. Lin, J. Segner, and G. Ertl, Surface Sci., 155 (1985), 101.
13. M. Karikorpi, S. Holloway, N. Henriksen, and J.K. Norskov, Surface Sci. 179, (1987), L41.
14. W. Van Willigen, Phys. Lett., 28A (1968), 80.
15. G. Wedler, K.P. Guess, K.G. Colb, and G. McElhiney, Appl. Surf. Sci., 1 (1978), 471.

FIGURE CAPTIONS

Figure 1: Angle resolved thermal desorption transients for desorption of deuterium from Fe(110) - detector located normal to surface. Deuterium exposure: A, 6.5L; B, 3.3L; C, 1.9L.

Figure 2: Angle resolved desorption transients for desorption of deuterium from Fe(110). Deuterium exposure = 6.5L. Detector angle relative to surface normal: A, 0°; B, 30°; C, 50°; D, 60°.

Figure 3: Summary of desorption flux as a function of detector angle relative to the surface normal for angle resolved thermal desorption of deuterium from Fe(110). Deuterium exposure: (•) 6.5L; (x) 522L.

Figure 4: Summary of thermal desorption transients for deuterium desorbing from Fe(110) along the surface normal for a range of initial exposures at 200K. Transients have been corrected for nonthermal velocity effects. Each curve is the average of three desorption measurements.

Figure 5: Comparison of results for deuterium adlayer coverage as a function of exposure of an Fe(110) surface to deuterium at 200K: (•) Angle resolved thermal desorption; (O) Helium-monitored thermal desorption.

Figure 6: Comparison of angle-resolved thermal desorption transient with results obtained by differentiation of helium scattering monitored desorption spectrum for a deuterium exposure of 3.3L. (●) Angle-resolved transient corrected for velocity effects; (x) helium monitored transient; (solid line) - fit to Equation 1.

Figure 7: Sticking coefficient for the adsorption of deuterium on Fe(110) as a function of adlayer coverage at T = 200K, derived from Figure 5.

Figure 8: Potential energy diagram for the dissociative adsorption of hydrogen or deuterium on Fe(110). Distances on the horizontal axis are arbitrary.

TABLE 1

ACTIVATION ENERGIES

TECHNIQUE	SPECIES	ENERGY
TDS	Deuterium	Desorption Energy (E_d)=27.3±1.8 pre-exponential (ν)=(5±2)X 10^{-3}cm²/molecule-sec
He TDS	Deuterium	E_d=26.4±1.2 kcal/mole ν=(5.1±1.7)x10^{-3}cm²/molecule-sec
Isothermal Desorption	Deuterium	E_d=26.1±1 kcal/mole ν=(8.1±2.3)x10^{-3}cm²/molecule-sec
Isosteres	Deuterium	Heat of adsorption (ΔH_a)=24.7±2.9 kcal/mole
Spatial Distribution (Van Willigen Model)	Deuterium	Activation energy for Adsorption (E_a)=580± 70 cal/mole
Spatial Distribution (Comsa & David Model)	Deuterium	E_a=710±80 cal/mole
He TDS	Hydrogen	E_d=25.2±1.5 kcal/mole ν=(1.9±0.4)x10^{-3}cm²/molecule-sec
Isothermal Desorption	Hydrogen	E_d=25.1±1.3 kcal/mole ν=(3.5±1.5)x10^{-3}cm²/molecule-sec
Isosteres	Hydrogen	ΔH_a=24.2±2.4 kcal/mole

FIGURE 1 : E.A. KUCZ ET AL. [illegible]

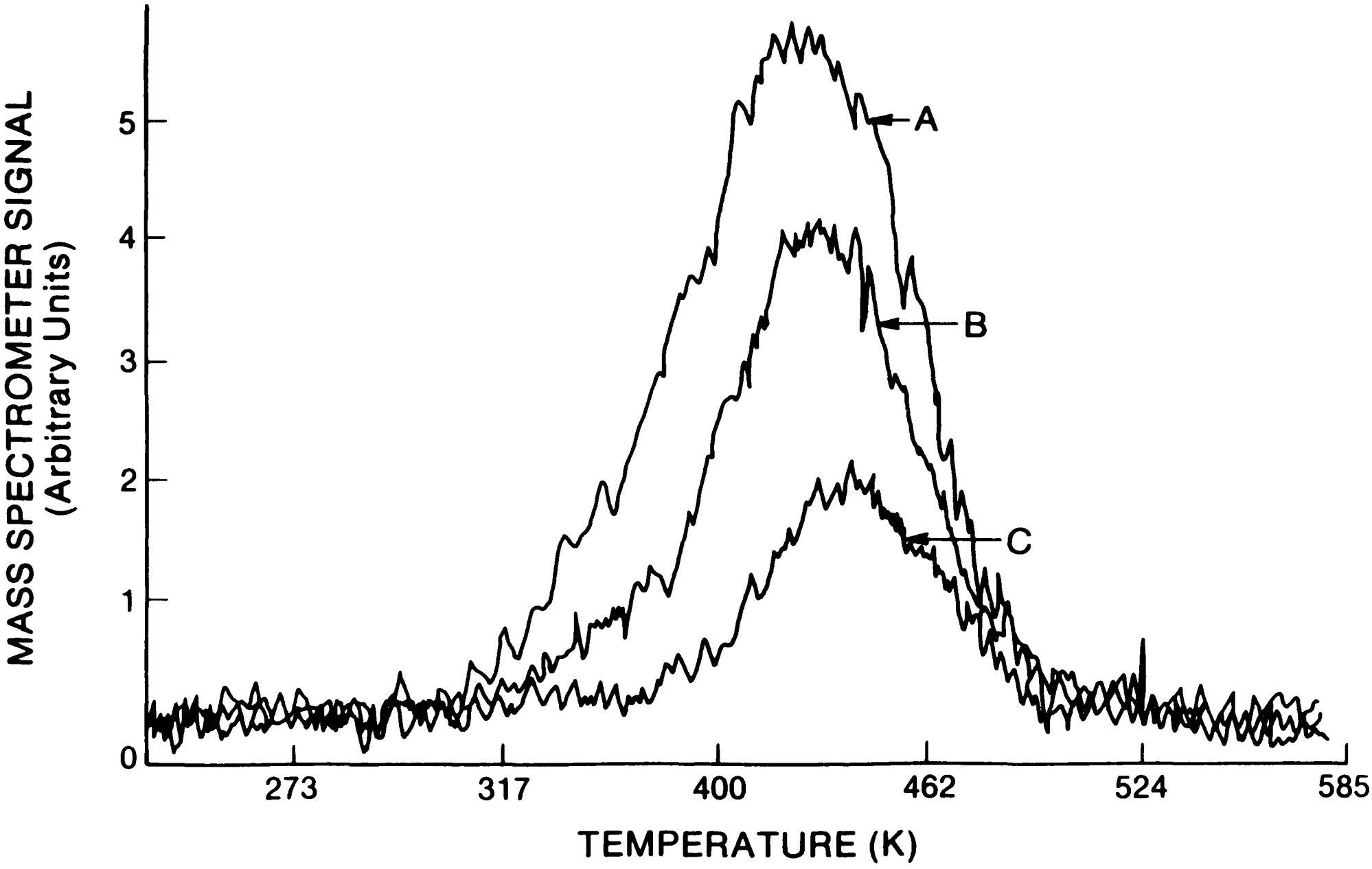

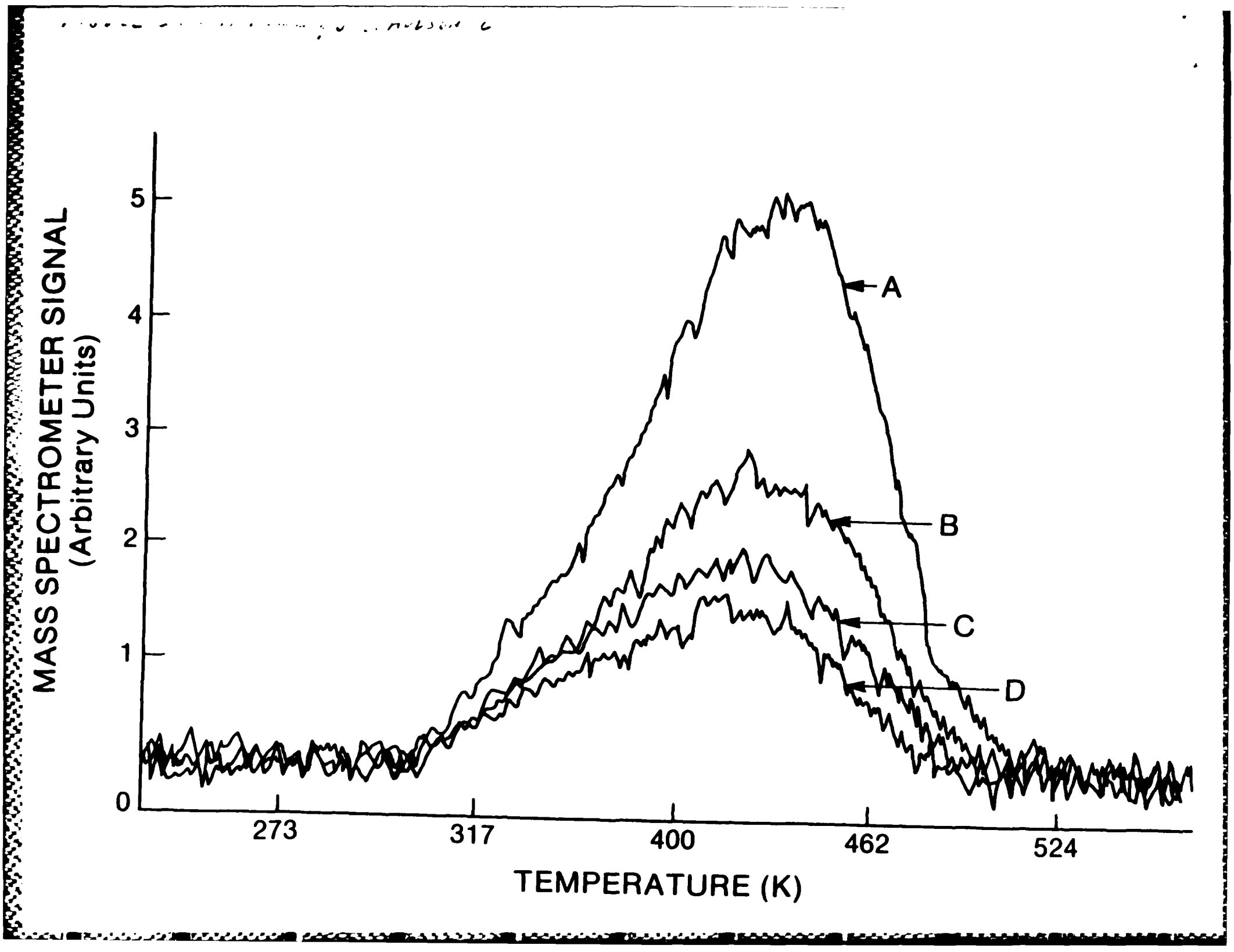
MASS SPECTROMETER SIGNAL
(Arbitrary Units)
5
4
3
2
1
0
A
B
C
D
273
317
400
462
524
TEMPERATURE (K)

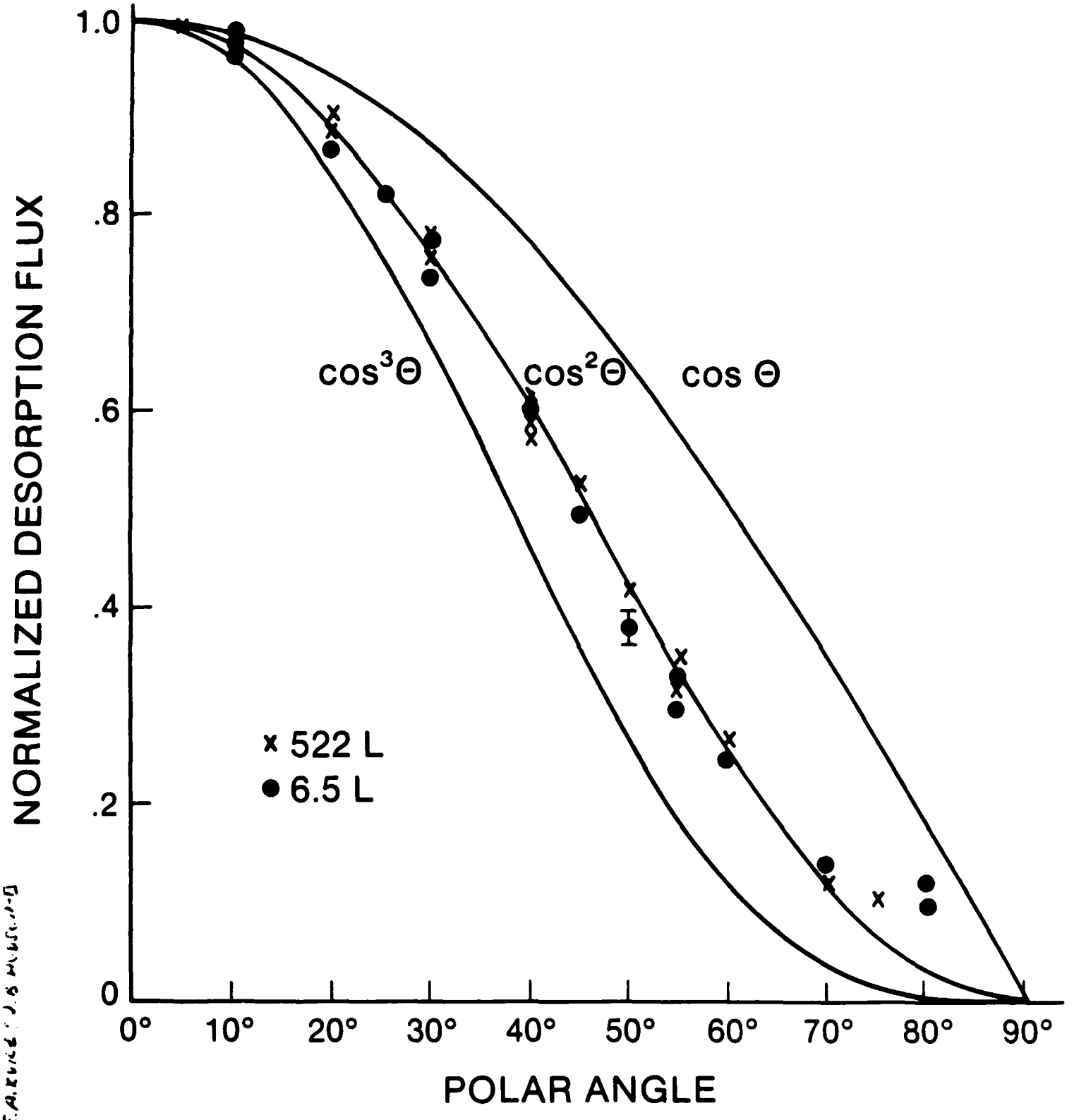
1.0
.8
.6
.4
.2
0
NORMALIZED DESORPTION FLUX
cos³Θ
cos²Θ
cos Θ
x 522 L
● 6.5 L
0°
10°
20°
30°
40°
50°
60°
70°
80°
90°
POLAR ANGLE

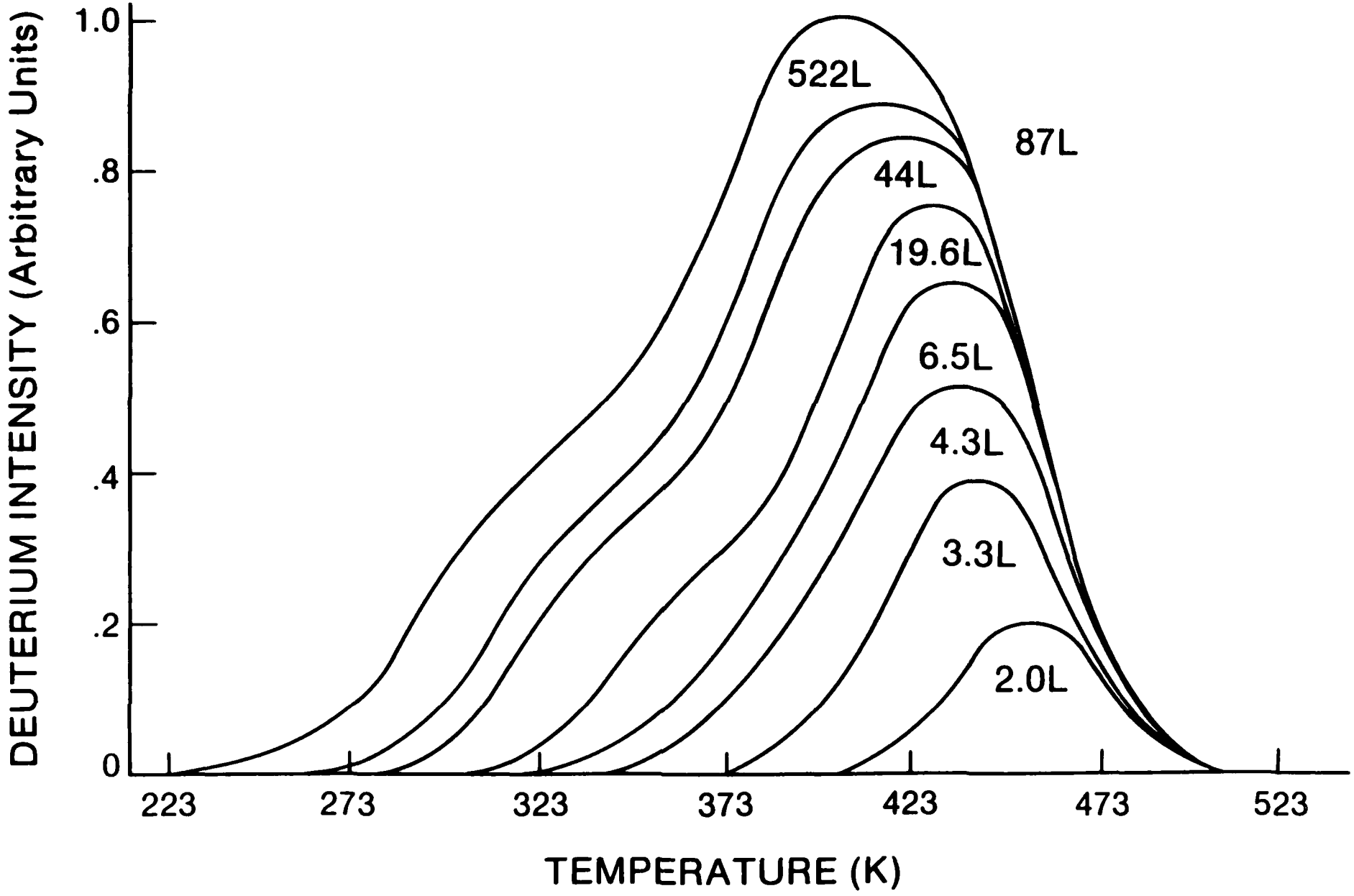
DEUTERIUM INTENSITY (Arbitrary Units)
1.0
.8
.6
.4
.2
0
522L
87L
44L
19.6L
6.5L
4.3L
3.3L
2.0L
223
273
323
373
423
473
523
TEMPERATURE (K)

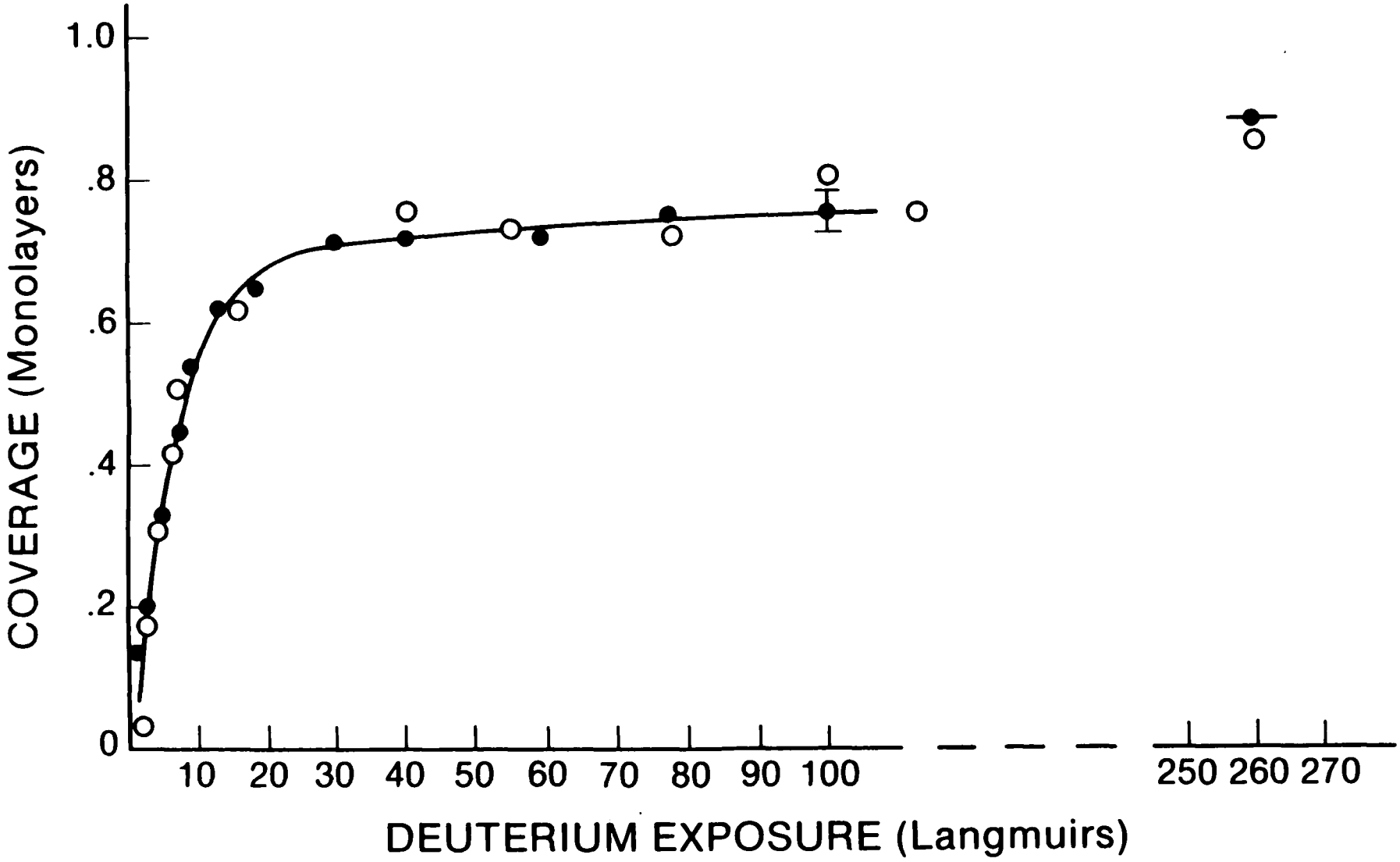
1.0
.8
.6
.4
.2
0
COVERAGE (Monolayers)
10 20 30 40 50 60 70 80 90 100
250 260 270
DEUTERIUM EXPOSURE (Langmuirs)

FIGURE 6 : E.H. KIM & J.B. NELSON - II

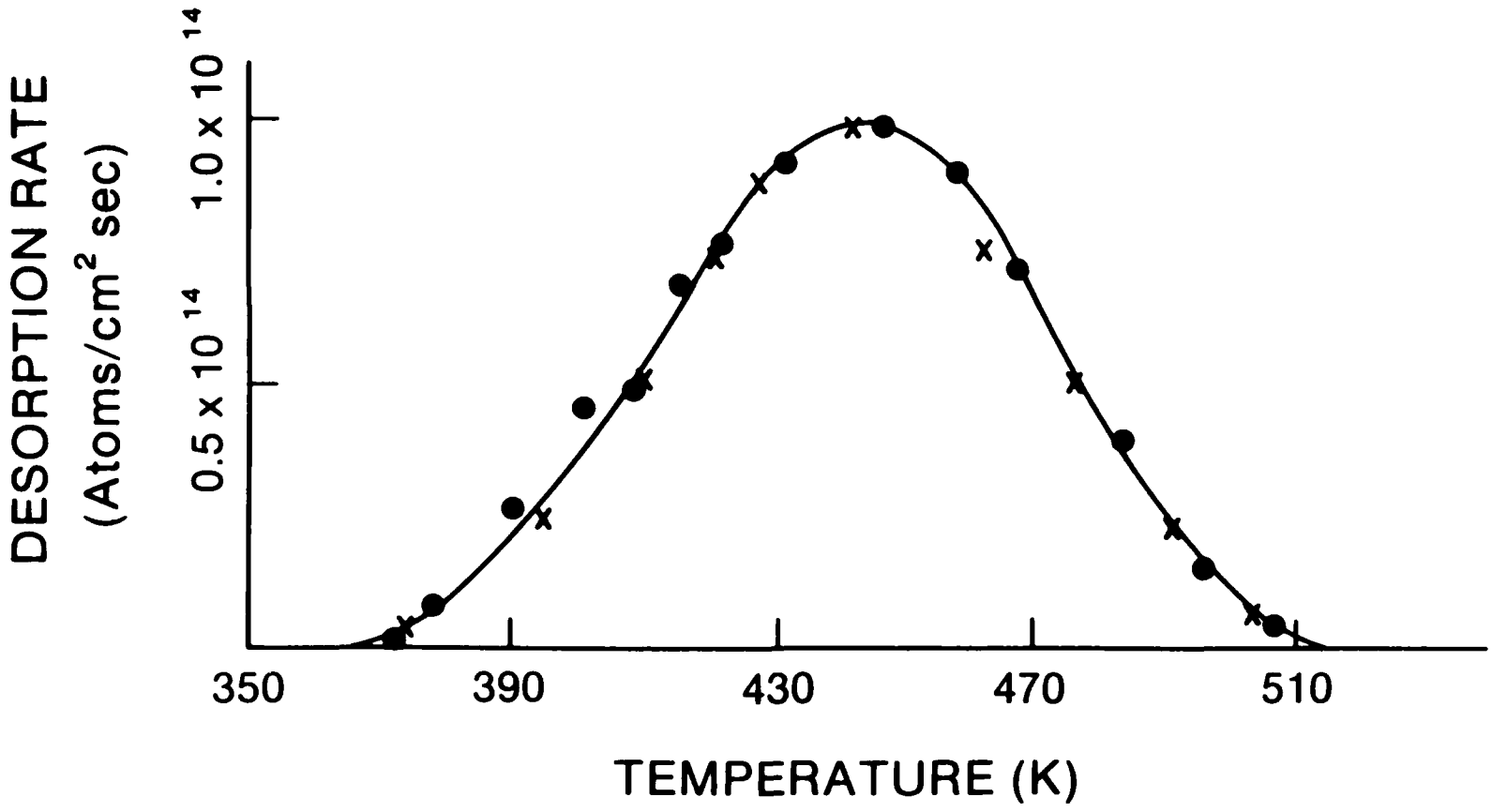

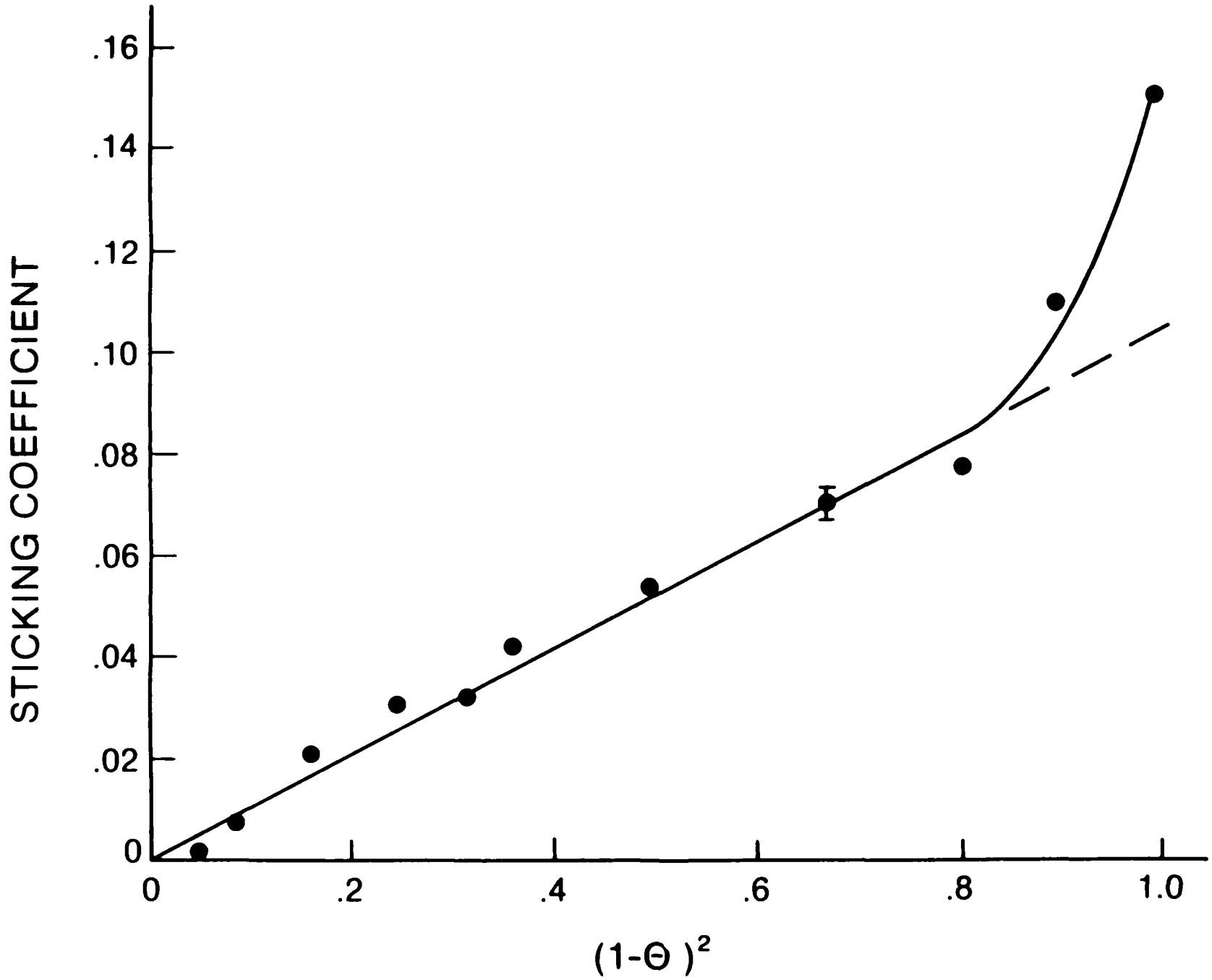
STICKING COEFFICIENT
.16
.14
.12
.10
.08
.06
.04
.02
0
0
.2
.4
.6
.8
1.0
(1-Θ)²

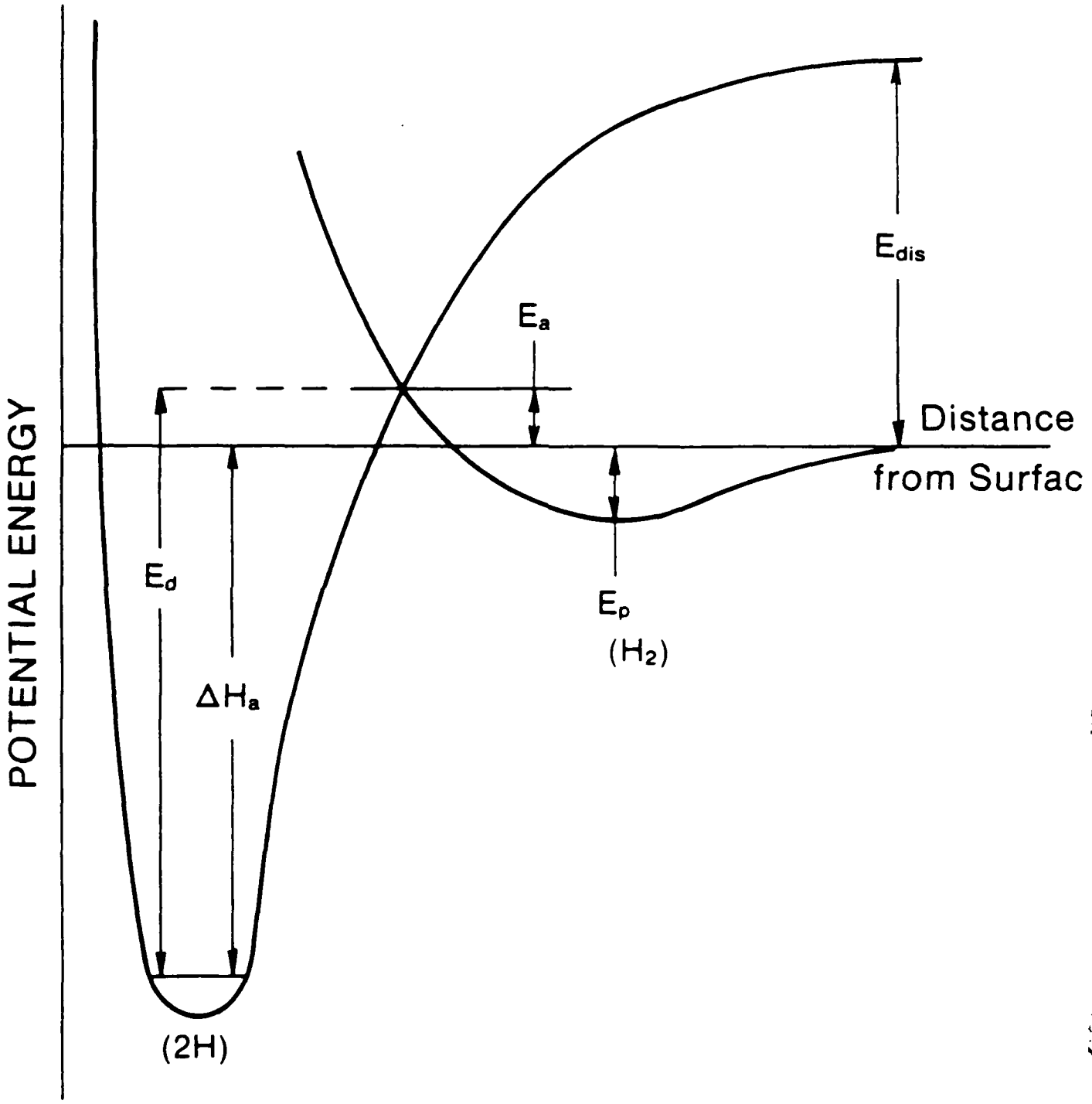
POTENTIAL ENERGY
Distance
from Surfac
E_{dis}
E_a
E_d
ΔH_a
E_p
(H_2)
(2H)

END

9-87

DTIC